Universal quantum control of two-electron spin quantum bits using dynamic nuclear polarization

Sandra Foletti[1]★, Hendrik Bluhm[1]★, Diana Mahalu[2], Vladimir Umansky[2] and Amir Yacoby[1]†

One fundamental requirement for quantum computation is to carry out universal manipulations of quantum bits at rates much faster than the qubit's rate of decoherence. Recently, fast gate operations have been demonstrated in logical spin qubits composed of two electron spins where the rapid exchange of the two electrons permits electrically controllable rotations around one axis of the qubit. However, universal control of the qubit requires arbitrary rotations around at least two axes. Here, we show that by subjecting each electron spin to a magnetic field of different magnitude, we achieve full quantum control of the two-electron logical spin qubit with nanosecond operation times. Using a single device, a magnetic-field gradient of several hundred millitesla is generated and sustained using dynamic nuclear polarization of the underlying Ga and As nuclei. Universal control of the two-electron qubit is then demonstrated using quantum state tomography. The presented technique provides the basis for single- and potentially multiple-qubit operations with gate times that approach the threshold required for quantum error correction.

The potential realization of quantum computers has attracted a lot of attention because of their promise to carry out certain calculations practically intractable for classical computers. Whereas a classical bit attains only two values (0 and 1), the phase space of a quantum bit (a two-level system) is in one-to-one correspondence with the points on the surface of a three-dimensional sphere, known as the Bloch sphere[1], where the basis states (corresponding to the classical 0 and 1) are represented at the north and south pole (Fig. 1a). A generic manipulation of the qubit needed to implement universal gate operations requires the ability to carry out rotations around two axes in the Bloch sphere[2–5] (for example, the z and x axis). In the present work, the two-level quantum bit (smallest logical unit of the quantum computer) is encoded in the spin state of two electrons confined in a double-well potential. This semiconductor-based system has the potential for good scalability, manipulations are all-electrical and potentially fast enough to enable 10^4 universal gate operations within the coherence time, an essential requirement for quantum error correction[6].

For two-electron spin qubits, rotations around the z axis, corresponding to the coherent exchange of two electrons, have recently been demonstrated[7]. Rotations around the second axis require the presence of a non-uniform magnetic field across the double-well potential, making the two spins precess at different rates. Here, we take advantage of the interaction of the electrons with the nuclear magnetic field of the Ga and As sublattices of the host material to generate the required magnetic-field gradient. Although fluctuations of this hyperfine field are known to be a principal source of decoherence[8–12], in this article we demonstrate the possibility of building up a gradient in the hyperfine field that significantly exceeds the fluctuations and can be sustained for times longer than 30 min. This is done by using pumping schemes that transfer spin and thus magnetic moment from the electronic system to the nuclei. Internally created gradients of nuclear field, in excess of 200 mT, together with the coherent exchange of the two electrons allow us to rapidly manipulate the two-electron spin qubit. The coherent manipulation is demonstrated by

reconstructing the evolution of the state within the Bloch sphere through quantum state tomography.

The double-well potential that confines the electrons is formed by applying a negative voltage to metal gates deposited on top of a two-dimensional electron gas embedded in a GaAs/AlGaAs heterostructure. The negative potential depletes the electrons underneath the metal gates, creating two isolated puddles of electrons (double quantum dot, Fig. 1b). The number of electrons in the dots can be controlled by tuning the potentials on the gates. We restrict the total occupation of the double quantum dot to two electrons, and describe their spatial separation by the parameter ε: for $\varepsilon \gg 0$, both electrons are in the right quantum dot, the (0, 2) configuration; for $\varepsilon \ll 0$, one electron occupies each dot, the (1, 1) configuration. The parameter ε and hence the dots' charge state can be continuously swept through intermediate configurations by varying the voltages on the metal gates. In the (0, 2) charge configuration, the only energetically accessible spin configuration is the singlet state $S(0,2) = (\uparrow\downarrow - \downarrow\uparrow)/\sqrt{2}$ (the arrows indicate the direction of the electron spins). As we separate the electrons, the wavefunctions' overlap decreases and four spin configurations become energetically degenerate: the singlet $S(1,1)$ and three triplets $T_0 = (\uparrow\downarrow + \downarrow\uparrow)/\sqrt{2}$, $T_- = \downarrow\downarrow$ and $T_+ = \uparrow\uparrow$ (Fig. 1d). We select the states $S(1,1)$ and T_0, both having zero z component of the spin angular momentum, as the basis states of our logical qubit[13,14] and lift the degeneracy with the states T_- and T_+ by applying an external magnetic field B_{ext}. The Zeeman energy $E_z = g\mu_B B$ ($g = -0.4$ is the g-factor for GaAs and μ_B is Bohr's magneton) shifts the T_+ state to lower energies, creating a crossing point with the singlet (marked by a red circle in Fig. 1d) at a value of ε that depends on $\mathbf{B} = \mathbf{B}_{ext} + \mathbf{B}_{nuc}$, where $\mathbf{B}_{nuc} \equiv (\mathbf{B}_{nuc,L} + \mathbf{B}_{nuc,R})/2$ is the average hyperfine field and $\mathbf{B}_{nuc,L}$ and $\mathbf{B}_{nuc,R}$ are the nuclear fields felt by the electron in the left and right dot, respectively (Fig. 1c). Within this logical subspace, rotations around the z axis are controlled by the energy splitting between $S(1,1)$ and T_0, denoted by $J(\varepsilon)$. This evolution amounts to a coherent exchange of the two electrons. Rotations around the x axis are controlled

[1]Department of Physics, Harvard University, Cambridge, Massachusetts 02138, USA, [2]Braun Center for Submicron Research, Department of Condensed Matter Physics, Weizmann Institute of Science, Rehovot 76100, Israel. *These authors contributed equally to this work.
†e-mail: yacoby@physics.harvard.edu
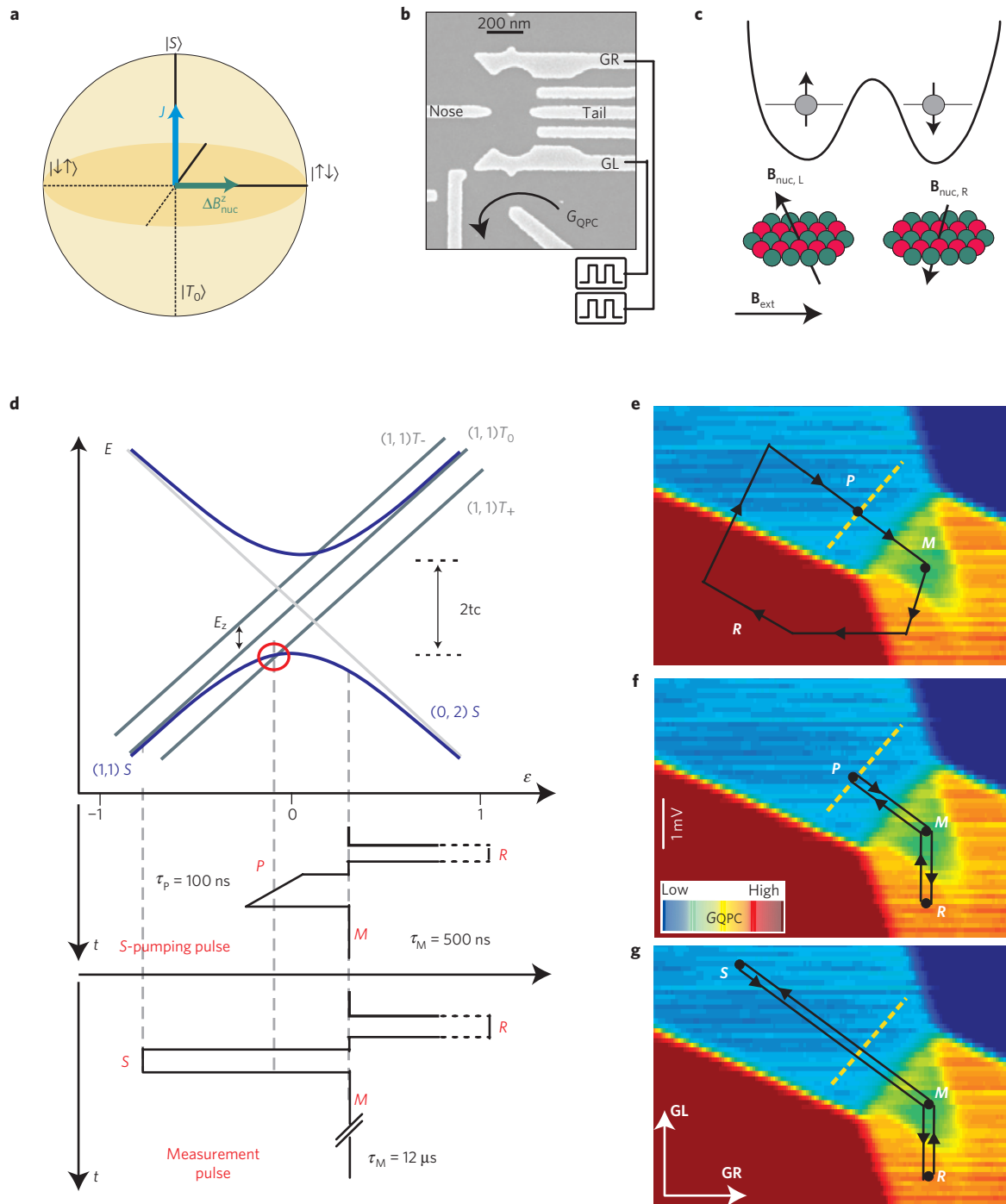
Figure 1 | Pump and measurement schemes. a, Geometrical representation (Bloch sphere) of the two-level system (S and T_0) and the two rotation axes (J and ΔB_{nuc}^z) allowing the implementation of universal single-qubit gates. **b**, SEM micrograph of a device similar to the one measured. Gates GL and GR control the charge configuration of the two dots; the central gates (Nose and Tail) control the tunnelling rate between the two dots. The average charge configuration is detected by measuring the conductance (G_{QPC}) through a capacitively coupled QPC. **c**, $\mathbf{B}_{nuc,L}$ and $\mathbf{B}_{nuc,R}$ are the local magnetic fields experienced by the electrons in the left and right dot through hyperfine coupling with the Ga and As nuclei. **d**, Schematic representation of the energy levels at the (0, 2)–(1, 1) charge transition for finite external magnetic field. The detuning ε from the degeneracy point is controlled by the voltages on GL and GR. Two pulse cycles are presented. (1) Nuclear pumping: the system is moved to point P where S and T_+ are degenerate and can mix. (2) Measurement pulse: the system is moved to large negative detuning where the states S and T_0 can mix. **e–g**, The T_+-pumping pulse scheme (**e**), the S-pumping pulse scheme (**f**) and the measurement pulse scheme (**g**), all shown as a function of GL and GR.

by the z component of a magnetic-field gradient across the two electrons, $\Delta\mathbf{B}_{nuc} = \mathbf{B}_{nuc,L} - \mathbf{B}_{nuc,R}$. If we thus let a state evolve around a combined axis $J\mathbf{z} + g\mu_B\Delta B_{nuc}^z\mathbf{x}$, the precession frequency will be given by $f = \sqrt{J^2 + (g\mu_B\Delta B_{nuc}^z)^2}/h$ ($h \approx 4 \times 10^{-15}$ eV s is Plank's constant).

Whereas controlled z rotations have previously been shown[7], controlled rotations around the x axis of the two-electron logical qubit have not been demonstrated so far. Clearly, the challenge is to provide a stable magnetic-field gradient across the two dots that exceeds the intrinsic nuclear fluctuations owing to the hyperfine
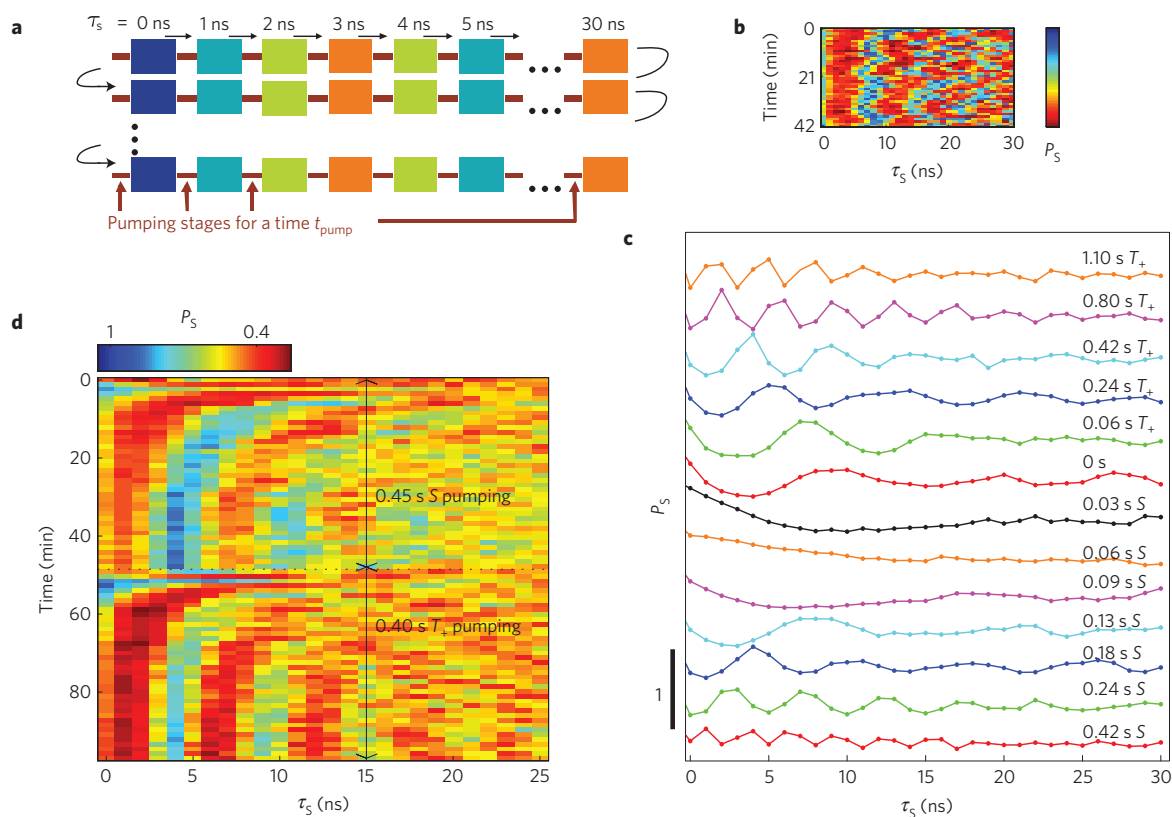
Figure 2 | Build-up of a gradient with two different pumping cycles. a, Schematic explaining the measurement of the singlet return probability as a function of τ_S. Each measurement point (rectangle) is an average over 1 s and preceded by a pump cycle that runs for a time t_{pump}. Each line is a repetition of the same measurement procedure. **b**, Measurement of the singlet return probability as a function of τ_S for $t_{pump} = 60$ ms. **c**, Singlet return probability as a function of separation time τ_S for different t_{pump}. Each data set line is an average over 30 τ_S sweeps. P_s is normalized by the size of the d.c. charge transition (see Supplementary Information). Traces are displaced for clarity. **d**, Crossover between S and T_+-pumping. The plot shows an average of nine subsequent repetitions of the same measurement. The disappearance of the oscillations on changing the pump pulse followed by a recovery (around 0 and 50 min) suggests that S and T_+-pumping produce ΔB_{nuc}^z of opposite sign. $B_{ext} = 1.5$ T for these data sets.
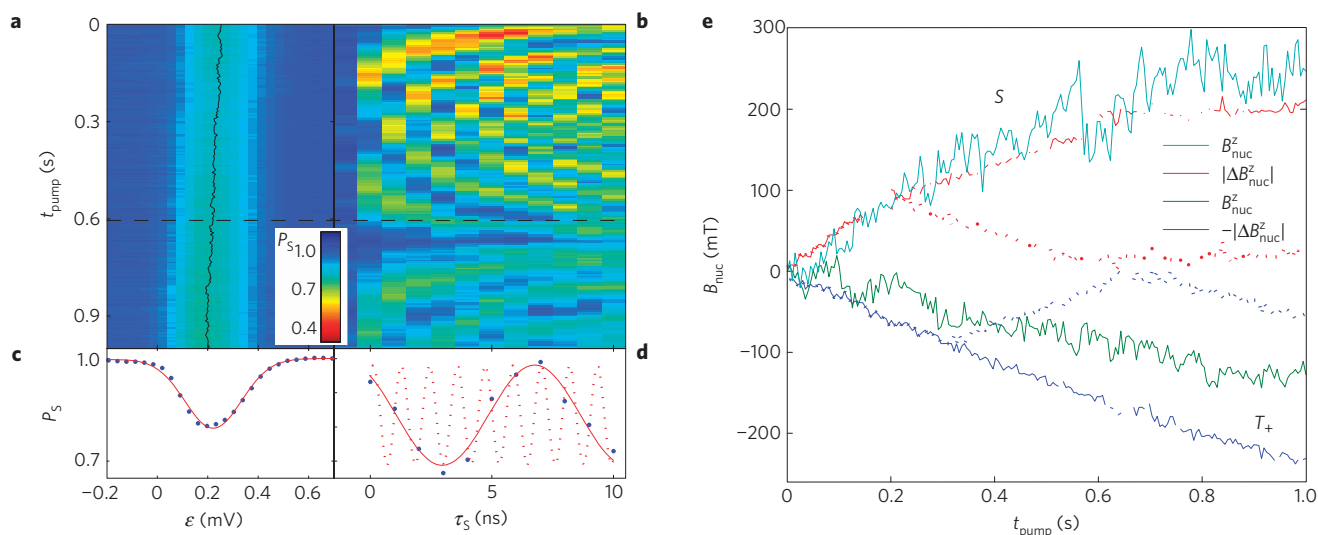
Figure 3 | Comparison of the gradient and the average nuclear field. a, Line scans of the position of the S–T_+ transition as a function of pump time: the T_+-pumping cycle, applied for a duration t_{pump}, precedes each 2-s-long measurement interval. **b**, Singlet return probability versus τ_S under the same pumping conditions as in **a**. The repeated increase and decrease of the apparent oscillation frequency is a consequence of aliasing of a monotonically increasing frequency because of the 1-ns sampling interval. **c**, Single line scan from the data in **a** at $t_{pump} = 0.6$ s. **d**, The corresponding τ_S sweep from **b**. The solid red line is a sinusoidal fit; the dashed line reconstructs the actual, non-aliased time dependence of the singlet probability. **e**, B_{nuc}^z and ΔB_{nuc}^z extracted from fits as shown in **c,d** as a function of t_{pump} for both T_+ and S-pumping. The shift of the S–T_+ transition was converted to B_{nuc}^z using its measured dependence on B_{ext} (see Supplementary Information)[16]; ΔB_{nuc}^z was obtained from the fitted oscillation frequency corrected for aliasing. The dotted lines show the same data before this correction. The fluctuations in the B_{nuc}^z curves reflect measurement noise. $B_{ext} = 500$ mT for these data sets.
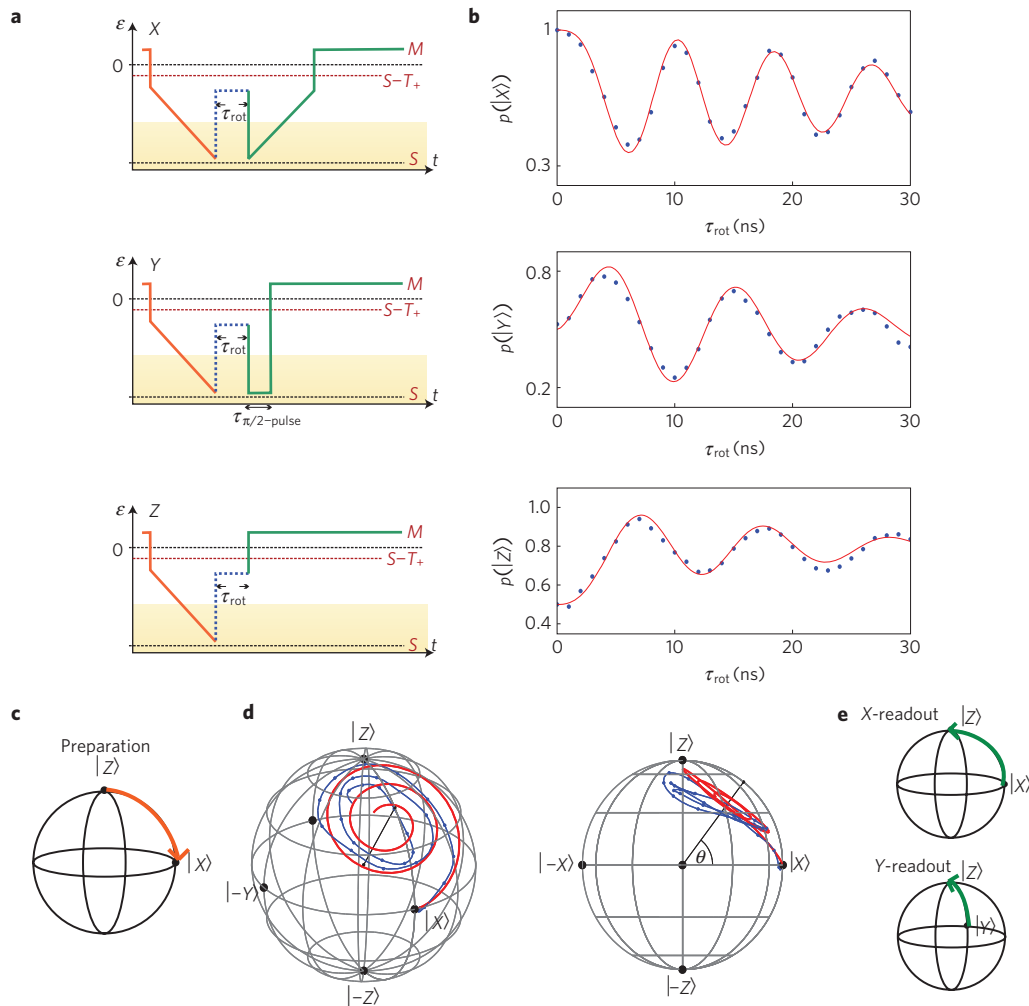
Figure 4 | State tomography and universal gate. a, Pulse schemes used to measure the singlet probability $p(|S\rangle) \equiv p(|Z\rangle)$, the $|\uparrow\downarrow\rangle$ probability $p(|\uparrow\downarrow\rangle) \equiv p(|X\rangle)$ and the $|S\rangle + i|T_0\rangle$ probability $p(|S\rangle + i|T_0\rangle) \equiv p(|Y\rangle)$ after rotation around a tilted, tunable axis. **b**, Measurements taken with the X, Y and Z pulses (dots) and fits (line) to a numerical solution of the Schrödinger equation of the S–T_0 Hamiltonian incorporating the finite pulse rise time and inhomogeneous broadening owing to fluctuations in ΔB_{nuc}^z. **c**, A $|\uparrow\downarrow\rangle = |X\rangle$ state is prepared by adiabatically turning off J. **d**, Representation of the measured and fitted trajectories in the Bloch sphere. To eliminate phase shifts owing to the slightly different frequencies (see text), the timescales for the X-data have been rescaled using spline interpolation so that the expected phase relations are maintained. The blue line is a spline interpolation of the data points in **b**. **e**, Visualization of the X and Y-readout schemes on the Bloch sphere.

interaction. Here, we present two polarization schemes by which the gradient can be increased to values significantly exceeding its fluctuations. Both pumping schemes make use of the degeneracy point between $S(1,1)$ and T_+. Transitions between the two states that are driven by the transverse component of $\Delta \mathbf{B}_{nuc}$ (ref. 15) are accompanied by a spin flip of the nuclei to conserve the total angular momentum. Our first pumping scheme follows a standard recipe[16,17] of initializing the system in the $S(0,2)$ state followed by a 50- or 100-ns-long sweep across the S–T_+ degeneracy point. This process ideally transfers one unit of angular momentum into the nuclear subsystem. In addition, we have developed an alternative pumping scheme, whereby we initialize the system in a $T_+(1,1)$ state followed by a similar slow passage through the S–T_+ degeneracy point. This new T_+-pumping scheme allows us to polarize the nuclear subsystem in a direction opposite to the S-pumping scheme. The T_+-pumping scheme works only when the Zeeman energy exceeds the electron temperature in the reservoirs: the system is swept slowly into (0, 1) and subsequently reloaded into the (1, 1) charge state (Fig. 1e). First the right and then the left electron align with the external field because of large Zeeman energy ($\approx$12.5 μeV at 500 mT), which preferentially loads a T_+ state.

Although the above nuclear pumping schemes should produce nuclear polarization, it is not obvious at all that this nuclear polarization should be different across the two dots[17]. As the mixing between the $S(1,1)$ and T_0 (1, 1) is sensitive only to the field gradient, we use a pulse cycle that monitors the coherent evolution around the x axis to measure this gradient. The system is first reset into a $S(0,2)$ state. ε is then abruptly set to point **S** in (1, 1) for an evolution time τ_S (see Fig. 1g). Here, $\Delta B_{nuc}^z \gg J(\varepsilon)/g\mu_B$ drives coherent oscillations between $S(1,1)$ and T_0 and the probability of being in a singlet state oscillates in time as $p(S) = \cos^2(g\mu_B \Delta B_{nuc}^z \cdot \tau_S/2\hbar)$. When the system is brought back to the measurement point **M**, only transitions from $S(1,1)$ to $S(0,2)$ are allowed, whereas T_0 remains blocked in the (1, 1) charge configuration. This spin-blockade effect allows mapping of the spin configuration of the state onto a charge configuration[18], which is measured by a charge sensor[18]. Here, we use a quantum point contact (QPC) positioned next to the double quantum dot (Fig. 1b) to detect changes in the double-dot charge configuration. The QPC signal, averaged over many gradient-probing cycles, is proportional to the probability of being in a singlet state.

A steady-state nuclear field can be achieved by continuously alternating between a pump cycle that runs for a time t_{pump}, and a gradient probing cycle that runs for 1 s, as schematically shown in Fig. 2a. In each measurement stage, a gradient probing pulse with a different separation time τ_S is used ($0 \leq \tau_S \leq 30$ ns for each τ_S sweep). The outcome of a measurement repeating τ_S sweeps 40 times and using $t_{pump} = 60$ ms is shown in Fig. 2b. An oscillatory signal with a frequency fluctuating around a steady mean is clearly visible. In the present measurement, the gradient is kept in a steady state for 40 min, but this time could have been extended indefinitely. Each curve in Fig. 2c shows an average over 30 τ_S sweeps and the different values of t_{pump} control the steady-state value of the gradient in each data set. We observe that the oscillations vanish (corresponding to a ΔB_{nuc}^z fluctuating around 0) at moderate S-pumping rather than $t_{pump} = 0$. This seems to reflect a small polarization effect from the measurement pulses that can be compensated with S-pumping (see Supplementary Information). To compare the S and T_+-pumping schemes, we have taken a measurement where we have switched between S-pumping and T_+-pumping every 40 τ_S sweeps (see Fig. 2c). The data show that on changing the pump cycle, the oscillations disappear and then recover after a few minutes in a way that suggests a sign change of the induced gradient.

Besides determining the magnitude of the gradient by means of coherent x rotations, we can also measure the average value of the nuclear field by monitoring the position of the S–T_+ transition[16]. This should clarify whether spins are flipped in only one or both dots. Figure 3a,b shows interleaved measurements of the position of the S–T_+ transition[17] and the oscillatory S–T_0 mixing as a function of t_{pump} using the T_+-pumping cycle. A shift of the S–T_+ transition to more negative ε corresponds to the build-up of an average field B_{nuc}^z oriented opposite to the external magnetic field, consistent with spin flips from down to up in the nuclear system[19]. Figure 3e shows that at $B_{ext} = 500$ mT, ΔB_{nuc}^z reaches 230 mT and B_{nuc}^z about 130 mT. The ratio of nearly a factor of two indicates that the nuclei are polarized predominantly in one of the two dots. Data obtained using the S-pumping cycle (Fig. 3e) show a ΔB_{nuc}^z that tends to be slightly smaller than the average field. The value of B_{nuc}^z can be subject to various systematic analysis errors, but it is clearly not much larger than ΔB_{nuc}^z (see Supplementary Information).

Combining our slowly tunable x-rotation gate with the electrically controllable exchange gate allows single-qubit rotations around an axis that can be rapidly tilted to any desired angle between 0 and nearly $\pi/2$ away from the x axis (angle θ in Fig. 4d). Concatenating rotations around different axes allows us to implement universal quantum control. We demonstrate and characterize the rotation around an arbitrary axis using state tomography, consisting of three independent measurements of the probability of being in a $|S\rangle \equiv |Z\rangle$, in a $|S\rangle + |T_0\rangle \equiv |\uparrow\downarrow\rangle \equiv |X\rangle$ and in a $|S\rangle + i|T_0\rangle \equiv |Y\rangle$ state[1], with pulses shown in Fig. 4a. This allows us to fully reconstruct the time evolution of the state vector. For each of the measurements, we first prepare a $|\uparrow\downarrow\rangle$ state by loading an $S(0,2)$ and adiabatically switching off $J(\varepsilon)$ in $(1,1)$. The desired rotation is carried out by quickly setting J to a finite value for a time τ_{rot}. Rapidly returning to $S(0,2)$ allows us to measure $p(|Z\rangle) \equiv |\langle Z|\psi\rangle|^2$, whereas slowly increasing J brings $|\uparrow\downarrow\rangle$ onto $|S\rangle$ and $|\downarrow\uparrow\rangle$ onto $|T_0\rangle$), thus allowing the readout of $p(|X\rangle) \equiv |\langle X|\psi\rangle|^2$. To obtain $p(|Y\rangle) \equiv |\langle Y|\psi\rangle|^2$, J is turned off for a time corresponding to a $\pi/2$ rotation around the x axis before rapidly returning to **M**. The results of this procedure for a particular choice of J and ΔB_{nuc}^z are shown in Fig. 4b as a function of τ_{rot}. For ideal pulses, one would expect $p(|X\rangle)$ to oscillate sinusoidally between 1 and $(1 + \cos(2\theta))/2$, and $p(|Z\rangle)$ between $1/2$ and $(1 + \sin(2\theta))/2$, whereas $p(|Y\rangle)$ should vary symmetrically around $1/2$. Deviations from this behaviour can be attributed to a finite pulse rise time and high-pass filtering of the pulses. The first causes an approximately adiabatic drift of the rotation axis that

prevents $p(|Z\rangle)$ from returning to the starting point, whereas the second leads to slightly different ε-offsets and thus different $J(\varepsilon)$ for different pulses, causing a $\approx 25\%$ frequency change. Fits to a model (see Supplementary Information) incorporating these effects and inhomogeneous broadening owing to fluctuations in ΔB_{nuc}^z give a good match with the data (Fig. 4b). In Fig. 4d, the data and fits are shown in the Bloch-sphere representation. We estimate that the errors owing to measurement noise, pulse imperfections other than those included in the model, incomplete ensemble averaging over nuclear fluctuations and uncertainties in the QPC conductance calibration (see Supplementary Information) are of the order of 0.15 for all three probability measurements. They could be substantially reduced by improving the characteristics of our high-frequency set-up, such that pulse compensation schemes would be simpler and pulse-dependent variations of J could be eliminated.

The mechanism responsible for the large gradient due to pumping is unknown at present. One possible cause is an asymmetry in the size of the two dots due to local disorder. Both the probability to flip a nuclear spin in one of the dots and the change in hyperfine field owing to that flip are inversely proportional to the number of nuclei N over which the electron wavefunction extends[20]. The overall $1/N^2$ dependence results in the smaller dot being polarized more rapidly. Different relaxation rates in the two dots and more complex aspects of the nuclear dynamics may also have a role[21]. The relationship between our results and those of Reilly et al.[17], where a strong suppression of ΔB_{nuc}^z was reported, is under investigation at present. The apparent contradiction with the observation in ref. 22 that S-pumping becomes ineffective at fields exceeding a few tens of millitesla might be due to a different coupling between the dots and to the electron reservoirs (see Supplementary Information).

We demonstrated the ability to carry out universal single-qubit operations in subnanosecond timescales[23], two orders of magnitude faster than previously shown for single spin qubits[24–26]. These short operation times together with the demonstrated coherence times of a few microseconds[7] and predicted coherence times of up to 100 μs (refs 27–29) suggest that the requirements for quantum error correction of two-electron spin qubits are within reach. Furthermore, our ability to record the magnetic-field gradient opens the way towards feedback control of the nuclear environment that would prolong T_2^* and thereby reduce the number of error-correcting pulses needed.

References

1. Nielsen, M. A. & Chuang, I. L. *Quantum Computation and Quantum Information* (Cambridge Univ. Press, 2000).
2. Levy, J. Universal quantum computation with spin-1/2 pairs and Heisenberg exchange. *Phys. Rev. Lett.* **89,** 147902 (2002).
3. Coish, W. & Loss, D. Exchange-controlled single-electron-spin rotations in quantum dots. *Phys. Rev. B* **75,** 161302 (2007).
4. Press, D., Ladd, T. D., Zhang, B. & Yamamoto, Y. Complete quantum control of a single quantum dot spin using ultrafast optical pulses. *Nature* **456,** 218–221 (2008).
5. Hanson, R. & Burkard, G. Universal set of quantum gates for double-dot spin qubits with fixed interdot coupling. *Phys. Rev. Lett.* **98,** 050502 (2007).
6. Aharonov, D. & Ben-Or, M. Fault-tolerant quantum computation with constant error rate. *SIAM J. Comput.* **38,** 1207–1282 (2008).
7. Petta, J. R. *et al.* Coherent manipulation of coupled electron spins in semiconductor quantum dots. *Science* **309,** 2180–2184 (2005).
8. Khaetskii, A. V., Loss, D. & Glazman, L. Electron spin decoherence in quantum dots due to interaction with nuclei. *Phys. Rev. Lett.* **88,** 186802 (2002).
9. Merkulov, I. A., Efros, A. L. & Rosen, M. Electron spin relaxation by nuclei in semiconductor quantum dots. *Phys. Rev. B* **65,** 205309 (2002).
10. Witzel, W. M. & Sarma, S. D. Quantum theory for electron spin decoherence induced by nuclear spin dynamics in semiconductor quantum computer architecture. *Phys. Rev. B* **74,** 035322 (2006).
11. Koppens, F. H. L. *et al.* Control and detection of singlet–triplet mixing in a random nuclear field. *Science* **309,** 1346–1350 (2005).

12. Zhang, W., Dobrovitki, V., Al-Hassanieh, K., Dagotto, E. & Harmon, B. Hyperfine interaction induced decoherence of electron spins in quantum dots. *Phys. Rev. B* **74**, 205313 (2006).
13. Lidar, D. A., Chuang, I. L. & Whaley, K. B. Decoherence-free subspace for quantum computation. *Phys. Rev. Lett.* **81**, 2594–2597 (1998).
14. Taylor, J. M. *et al.* Fault-tolerant architecture for quantum computation using electrically controlled semiconductor spins. *Nature Phys.* **1**, 177–183 (2005).
15. Taylor, J. M. *et al.* Relaxation, dephasing, and quantum control of electron spins in double quantum dots. *Phys. Rev. B* **76**, 035315 (2007).
16. Petta, J. R. *et al.* Dynamic nuclear polarization with single electron spins. *Phys. Rev. Lett.* **100**, 067601 (2008).
17. Reilly, D. J. *et al.* Suppressing spin qubit dephasing by nuclear state preparation. *Science* **321**, 817–821 (2008).
18. Johnson, A. C. *et al.* Triplet–singlet spin relaxation via nuclei in a double quantum dot. *Nature* **435**, 925–928 (2005).
19. Paget, D., Lampel, G. & Sapoval, B. Low field electron–nuclear spin coupling in gallium arsenide under optical pumping conditions. *Phys. Rev. B* **15**, 5780–5796 (1977).
20. Stopa, M., Krich, J. J. & Yacoby, A. Inhomogeneous nuclear spin flips. Preprint at <http://arxiv.org/abs/0905.4520v1> (2009).
21. Maletinsky, P., Badolato, A. & Imamoglu, A. Dynamics of quantum dot nuclear spin polarization. *Phys. Rev. Lett.* **99**, 056804 (2007).
22. Reilly, D. J. *et al.* Exchange control of nuclear spin diffusion in double quantum dots. Preprint at <http://arxiv.org/abs/0803.3082v1> (2008).
23. Greilich, A. *et al.* Ultrafast optical rotations of electron spins in quantum dots. *Nature Phys.* **5**, 262–266 (2009).
24. Koppens, F. H. L. *et al.* Driven coherent oscillations of a single electron spin in a quantum dot. *Nature* **442**, 766–771 (2006).
25. Novack, K. C., Koppens, F. H. L., Nazarov, Y. V. & Vandersypen, L. M. K. Coherent control of a single electron spin with electric fields. *Science* **318**, 1430–1433 (2007).
26. Pioro-Ladriere, M. *et al.* Electrically driven single electron spin resonance in a slanting Zeeman field. *Nature Phys.* **4**, 776–779 (2008).
27. Yao, W., Liu, R. B. & Sham, L. J. Theory of electron spin decoherence by interacting nuclear spins in a quantum dot. *Phys. Rev. B* **74**, 195301 (2006).
28. Cywinski, L., Witzel, W. M. & Das Sarma, S. Electron spin dephasing due to hyperfine interactions with a nuclear spin bath. *Phys. Rev. Lett.* **102**, 057601 (2009).
29. Coish, W., Fischer, J. & Loss, D. Exponential decay in a spin bath. *Phys. Rev. B* **77**, 125329 (2008).

Author contributions

S.F. fabricated the samples. H.B developed the measurement software. Electron-beam lithography and sample growth were carried out by D.M. and V.U., respectively. S.F., H.B. and A.Y. planned and carried out the experiment, analysed the data and co-wrote the paper.

Additional information

Supplementary information accompanies this paper on www.nature.com/naturephysics. Reprints and permissions information is available online at http://npg.nature.com/reprintsandpermissions. Correspondence and requests for materials should be addressed to A.Y.